J. Fluid Mech. (2011), *vol.* 674, *pp.* 464–488.
doi:10.1017/S0022112011000097

Inviscid critical and near-critical reflection of internal waves in the time domain

ALBERTO SCOTTI†

Department of Marine Sciences, University of North Carolina, Chapel Hill, NC 27599, USA

(Received 19 May 2010; revised 29 November 2010; accepted 1 January 2011;
first published online 14 March 2011)

A solution that describes the inviscid reflection of internal waves off a sloping bottom in time is derived under conditions of linearity and uniform stratification. The solution is well behaved even under critical conditions. In the region $ky < Nt$, where k is the along-slope wavenumber of the incoming wave, y is the slope-normal direction, N is the Brünt–Väisälä frequency and t is time, an approximation can be written in terms of Lommel's function of two variables. The analysis can easily be extended to the case of a beam of finite width. In the non-critical case, the streamfunction relaxes to the classical Phillips steady-state solution in the region $y < c_g t$, where c_g is the slope-normal component of the group velocity for waves at the forcing frequency. However, it is found that the region where the along-boundary component of the velocity relaxes to the Phillips solution is also bounded from below, leaving a region very close to the wall where the classical solution misses important elements of the reflection process. This leads to interesting properties near the boundary, especially relatively to the formation of shear-driven unstable conditions.

Key words: internal waves, stratified flows

1. Introduction

Due to their peculiar dispersion relationship, the reflection of internal waves off a sloping boundary increases the local energy density and can lead to wave breaking and enhanced mixing (Staquet & Sommeria 2002). Field measurements have documented increased turbulent mixing two to three orders of magnitude above interior values over slopes (Moum *et al.* 2002; Nash *et al.* 2004) that can be traced to internal tide processes. In addition, the boundary mixing caused by internal tides and waves can generate mixed layers that diffuse away from oceanic slopes into the ocean interior, leading to density layering and seaward transport of particulate matter (Cacchione & Drake 1986; McPhee-Shaw & Kunze 2002; McPhee-Shaw 2006). Large turbulent shear in the bottom boundary layer can also have significant effects on the seabed. Cacchione, Pratson & Ogston (2002) proposed that increased bottom turbulence associated with critical semi-diurnal internal tides controls the shape and gradients of most continental slopes around the world's ocean basins. The enhanced turbulent shears essentially inhibit settlement of fine particles onto the bottom, thus controlling the long-term rates and loci of sediment accumulation on continental slopes. When the bed shear stresses owing to this process are high, resuspension and dispersion of suspended sediment away from the bottom boundary layer can occur as nepheloid

† Email address for correspondence: ascotti@unc.edu

layers (Dickson & McCave 2002; McPhee-Shaw & Kunze 2002). There also have been studies that link internal wave-induced bottom mixing to increased local biological productivity (MacIntyre 1998). Enhanced mixing caused by breaking and overturns in the bottom boundary layer for near-critical and critical internal waves has been observed in the laboratory (Cacchione & Wunsch 1974; Ivey & Nokes 1989; McPhee-Shaw & Kunze 2002; Gostiaux *et al.* 2006) and in numerical experiments (Slinn & Riley 1998; Legg & Adcroft 2003; Venayagamoorthy & Fringer 2006).

It should not be surprising then that great importance is attached to a theoretical understanding of the reflection process. The problem has been traditionally approached in the frequency domain (see e.g. Phillips 1966; Wunsch 1968; Thorpe 1987; Tabaei, Akylas & Lamb 2005), and for simplicity, in what follows, we will consider only two-dimensional waves in a non-rotating environment. For a given (real) frequency ω, the streamfunction of the waves is written as $\mathrm{e}^{\mathrm{i}\omega t}\psi(\omega, x, y)$. However, due to the nature of the equation which the streamfunction satisfies, this approach fails whenever the slope γ of the boundary coincides with the angle α that the group velocity of the incoming waves makes with the horizontal, the latter satisfying

$$\sin\alpha = \frac{\omega}{N}, \tag{1.1}$$

where N is the Brünt–Väisälä (assumed uniform). This failure is due the hyperbolic nature of the equation which $\psi(\omega, x, y)$ satisfies (Sobolev 1954; Wunsch 1969; Arnold & Khesin 1998). Along a critical slope the domain coincides with the characteristic lines of the equation, and the problem becomes ill-posed. The result is a divergent behaviour of the physical quantities described by the solution as the angle of the boundary approaches the critical value. This is at odd with experimental and observational evidence which show that at or near criticality, before turbulence sets it, the flow is well behaved (Cacchione & Wunsch 1974; De Silva, Imberger & Ivey 1997; Cacchione *et al.* 2002; Gostiaux *et al.* 2006), suggesting the existence of a mechanism that prevents the singularity from developing. The 'usual suspects' are viscosity and nonlinearity. The former was in fact used by Wunsch (1969) and Kistovich & Chashechkin (1995), while the latter was used more recently by Dauxois & Young (1999). Crucially, the latter authors, here referred to as DY, approached the problem in the time domain, as an initial/boundary value problem, rather than a boundary value problem for a steady state at a given frequency. The present paper follows the same approach, as we develop a theory for the reflection of *inviscid* and *linear* internal waves in the time domain. Unlike DY, we only assume linearity *a priori* and derive a solution for the linear reflection of a plane wave off a slope of an arbitrary angle. Note that both DY and Tabaei & Akylas (2003) show that to leading order dispersive effects dominate over nonlinear terms in the equation that controls the evolution of the streamfunction at the forcing frequency. Hence, working within a linear framework in the time domain is not as severe a constraint as it may appear, though it avoids the singularities that plague the approach in the frequency domain at criticality. We identify a similarity variable δ that measures, in an appropriate sense, proximity to the boundary, and we derive the non-trivial limit $\delta \to 0$ of the streamfunction in terms of functions well known in classical optics. The limit describes the evolution of the reflected wave in the near-wall region $\delta \ll 1$, free of singularities, indeed with an analytic dependence on the parameter measuring departure from criticality. Several interesting, and sometime counterintuitive properties of the reflection process in the linear and inviscid case emerge from this analysis. For example, in the critical case,

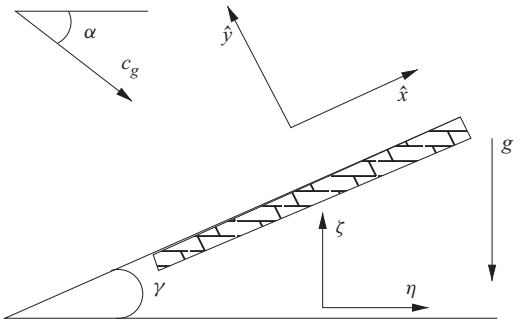

FIGURE 1. Sketch of the domain employed. The boundary, which extends to infinity in both directions, slopes upward at an angle γ. The group velocity c_g of the incoming wave makes an angle α with the horizontal. Angles are measured counterclockwise from the horizontal. Hence, for a downward propagating wave, $\alpha < 0$.

we show that if the incoming wave is a beam of finite width, the velocities within the domain are bounded in time, except at the boundary, where they grow linearly. Thus, deprived of the most egregious singularities, the present theory can be used as a basis to include the effects of nonlinear wave–wave interaction, identifying regions of instability and overturning, etc.

The rest of the paper is organized as follows: in § 2 we formulate the problem as an initial value/boundary value problem, solved with the aid of the Laplace transform; in § 3 we provide a non-trivial asymptotic expression for the inverse Laplace transform that provides the solution within the near-wall region, followed by a section in which we explore analytically the relationship between the evolving solution derived earlier with the classical solution derived by Phillips (1966); we then show how, using the superposition principle, it is possible analytically to localize the solution as a beam of finite width, which is how internal waves usually appear in experiments and in the field. With this solution, we explore the development of potentially unstable regions, either due large shear or statically unstable local stratification. A discussion and summary concludes the paper. Technical elements of the analysis are presented in appendices.

2. Analysis

2.1. *Mathematical formulation*

We consider a two-dimensional internal wave beam of the type studied by Tabaei & Akylas (2003), propagating in an inviscid fluid with constant Brunt–Väisälä frequency N under the Bousinnesq approximation. The beam approaches and reflects off a smooth surface making an angle γ (positive upward) to the horizontal. Even though in the ocean γ is typically small, we will not make *a priori* assumptions on its magnitude.

We perform the analysis in coordinates rotated so that $\hat{x}$ is parallel and $\hat{y}$ is normal to the boundary (figure 1). Under these assumptions, from the linearized Euler equations, it is easy to derive the following equation for the reflected streamfunction Ψ (Phillips 1966; Thorpe 1987):

$$\frac{\partial^2}{\partial \hat{t}^2}\nabla^2\Psi = -N^2\left(\cos\gamma\frac{\partial}{\partial\hat{x}} - \sin\gamma\frac{\partial}{\partial\hat{y}}\right)^2\Psi, \tag{2.1}$$

with the following initial conditions:

$$\Psi(\hat{x}, \hat{y}, \hat{t} = 0) = 0, \qquad \frac{\partial}{\partial \hat{t}}\Psi(\hat{x}, \hat{y}, \hat{t} = 0) = 0, \tag{2.2}$$

while at the boundaries

$$\Psi(\hat{x}, \hat{y} \to \infty, \hat{t}) = 0, \qquad \Psi(\hat{x}, \hat{y} = 0, \hat{t}) = \mathscr{A}(\hat{t})S(\hat{x})\,\mathrm{e}^{\mathrm{i}N\hat{t}\sin\alpha}. \tag{2.3}$$

The boundary condition at the wall assumes that the incoming wave is monochromatic in time with frequency $N\sin\alpha$ and $0 \leqslant \mathscr{A}(\hat{t}) \leqslant 1$ is a ramp-up/ramp-down function which accounts for dispersive effects at the leading edge of the incoming beam. To represent a internal wave beam of width $2L$, we assume that

$$S(\hat{x}) = A\frac{\mathrm{e}^{\mathrm{i}\hat{k}\hat{x}}}{1 + \left(\dfrac{\hat{x}}{\hat{L}}\right)^2}, \tag{2.4}$$

In view of the linearity of the problem, we will first seek the solution in the limit $L \to \infty$ and then use the superposition principle to generate the solution in the $L < \infty$ case.

2.2. *Solution strategy*

For an infinite beam, we seek a solution having the form $\Psi = \mathrm{e}^{\mathrm{i}\hat{k}\hat{x}}\psi(\hat{y}, \hat{t})$. The Laplace transform of ψ,

$$\psi(\hat{y}, \hat{p}) = \mathscr{L}[\psi] \equiv \int_0^\infty \psi(\hat{y}, \hat{t})\,\mathrm{e}^{-\hat{p}\hat{t}}\,\mathrm{d}\hat{p}, \tag{2.5}$$

satisfies the boundary value problem

$$\left[-\hat{k}^2(\hat{p}^2 + N^2\cos^2\gamma) + (\hat{p}^2 + N^2\sin^2\gamma)\frac{\partial^2}{\partial\hat{y}^2} - 2\mathrm{i}\hat{k}N^2\cos\gamma\sin\gamma\frac{\partial}{\partial\hat{y}}\right]\psi = 0, \tag{2.6}$$

with boundary conditions given by

$$\psi(\hat{y} = 0, \hat{p}) = \mathscr{L}[A(\hat{t})\exp(\mathrm{i}N\hat{t}\sin\alpha)] \equiv \psi_0(\hat{p}), \quad \lim_{\hat{y}\to\infty}\psi = 0. \tag{2.7}$$

The solution to the above problem must be found on the strip $\mathrm{Re}\,p > M$ with $M > 0$ chosen such that $\psi(\hat{p}, \hat{y})$ is holomorphic on it. In view of the linearity of the problem, the solution is given by

$$\psi(\hat{p}, \hat{y}) = \psi_0(\hat{p})\,\mathrm{e}^{\lambda(\hat{p})\hat{k}\hat{y}}, \tag{2.8}$$

where $\lambda(\hat{p})$ is the root of the characteristic equations associated with (2.6) which satisfies $\mathrm{Re}\,\hat{k}\lambda(\hat{p}) < 0$ for $\mathrm{Re}\,\hat{p}$ sufficiently large (the possibility of both roots having $\mathrm{Re}\,\hat{k}\lambda(\hat{p}) > 0$ when $\mathrm{Re}\,\hat{p} \gg N$ is ruled out by a trivial application of the fundamental theorem of algebra).

We assume that $\hat{k} > 0$, consistent with incoming waves with downward group velocity, and use the along-slope wavenumber $\hat{k}$ of the incoming wave and N to non-dimensionalize the problem by introducing the following non-dimensional variables $y \equiv \hat{k}\hat{y}$, $p \equiv \hat{p}/N$ and $t \equiv N\hat{t}$. Thus, this selects the root λ with negative real part.

Applying the inverse Laplace transform gives the solution in physical coordinates

$$\psi(y, t) = \frac{1}{2\pi\mathrm{i}}\int_{c-\mathrm{i}\infty}^{c+\mathrm{i}\infty}\psi(p, y)\,\mathrm{e}^{pt}\,\mathrm{d}p = \frac{1}{2\pi\mathrm{i}}\int_{c-\mathrm{i}\infty}^{c+\mathrm{i}\infty}\psi_0(p)\,\mathrm{e}^{\phi(p,y,t)}\,\mathrm{d}p, \tag{2.9}$$

where

$$\phi(p, y, t) = \lambda(p)y + pt. \tag{2.10}$$

The constant c in the integration contour is arbitrary, provided the integrand is holomorphic in the region $\mathrm{Re}\, p > c$. In practice, it is extremely convenient to extend ϕ, that is $\lambda(p)$, to the entire complex plane minus an appropriately chosen branch cut. There is a certain freedom in how to perform such extension, which can be used to simplify the analysis in different regions of the (y, t) plane. A detailed discussion of the extensions is presented in Appendix A.

2.3. *Initial set-up*

The ramp-up function $\mathscr{A}(t)$ depends on the details of the generation process of the incoming wavetrain, as well as on the dispersion of the wavefront over the travel time. To simplify the classification of the behaviour, we consider two possibilities: a hard ramp-up, whereby $\mathscr{A}(t)$ raises in a vanishingly small time from zero to 1 at $t = 0$, and a soft ramp-up, in which the ramp-up occurs linearly over a finite time τ. In practice, the hard ramp-up will be appropriate for a wave whose switch-on time scale τ is of the order of a buoyancy period, whilst the soft ramp-up will be more appropriate for waves such that $1 \ll \tau \ll 1/\sin\alpha$. In the former case

$$\psi_0^h(p) = \frac{1}{p - \mathrm{i}\sin\alpha}, \tag{2.11}$$

whereas in the latter

$$\psi_0^s(p) = \frac{1 - \exp[-(p - \mathrm{i}\sin\alpha)\tau]}{\tau(p - \mathrm{i}\sin\alpha)^2}. \tag{2.12}$$

Notice however that if $\psi^h(y, t)$ is the solution under the hard ramp-up condition, the solution under the soft ramp-up condition is

$$\psi^s(y, t) = \frac{1}{\mathrm{i}\tau}\left(\frac{\partial\psi^h(y, t)}{\partial\sin\alpha} - \frac{\partial\psi^h(y, t-\tau)}{\partial\sin\alpha}\,\mathrm{e}^{\mathrm{i}\tau\sin\alpha}H(t-\tau)\right), \tag{2.13}$$

where $H(t)$ is the Heaviside step function, and thus the soft ramp-up case can easily be obtained once the solution under hard ramp-up is known. For this reason, we focus on the hard ramp-up case and drop the superscript 'h' in what follows.

3. The streamfunction in the near field

It is easy to show (see Appendix B) that when $y > t$ the streamfunction decays exponentially in y, which is to be expected on physical grounds. In this section we will focus on the dynamically interesting near-field region $y < t$, with the goal of constructing a non-trivial approximation to (2.9) that captures the formation of the reflected wave.

3.1. *The near-field region, $y < t$*

To find a useful approximation for the streamfunction in the near-wall region, we set in (2.10) $\lambda \equiv \lambda_{nf}(p)$ with $\lambda_{nf}(p)$ defined in (A 3). We then deform the integration contour to coincide with the one shown in figure 2, along which the only non-zero contributions come from the contours along each side of the branch cuts (I_1 to I_4), and from the circular path centred on the origin C, whose radius is such to include the singularities at $-\mathrm{i}\sin\gamma$ and $\mathrm{i}\sin\alpha$ (the contribution from the outer arches tends

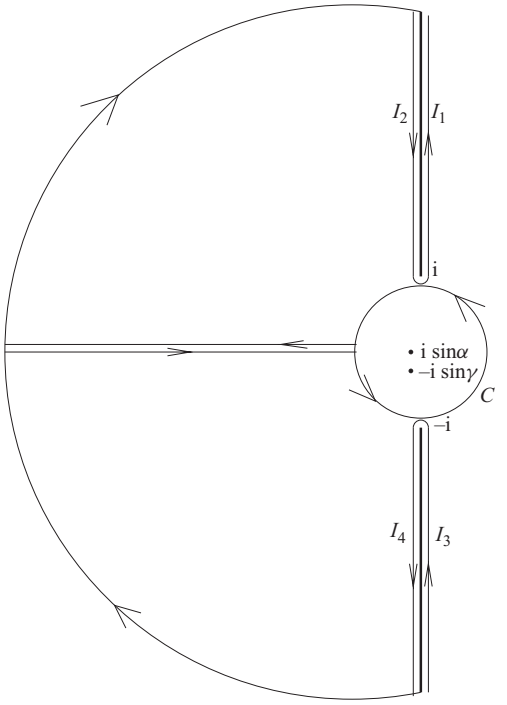

FIGURE 2. The integration contour for the near-field case. The branch cut stretches from i to $+\mathrm{i}\infty$ and from $-\mathrm{i}\infty$ to $-\mathrm{i}$. The contribution along the external arches vanishes as $1/R$, where R is the radius of the circle. Likewise, the contributions from the opposing paths across the real negative axis cancel each other as the distance between the paths is set to zero. Only the internal circle C and the four integrals I_1 to I_4 hugging the branch cuts give a non-zero contribution, of which the one along C is dominant in the near-wall region.

to zero as R^{-1}, with R being the radius of the arch), i.e.

$$\psi = \psi_C + \sum_{n=1}^{4} \psi_{I_n}. \tag{3.1}$$

It is on

$$\psi_C = \frac{1}{2\pi\mathrm{i}} \int_C \frac{\mathrm{e}^{\phi(p,y,t)}}{p - \mathrm{i}\sin\alpha}\,\mathrm{d}p \tag{3.2}$$

that we focus our attention here, since, as will be shown presently, it determines the response of the solution at the forcing frequency. The goal is to obtain a manageable non-trivial approximation to the streamfunction that captures the development of the reflected wave. The derivation below emphasizes the physical aspects. A formal derivation, starting from an exact representation of the integral along C as a series of Lommel's function is presented in Appendix C.

$\phi(p, y, t)$ has a simple pole at $-\mathrm{i}\sin\gamma$ (see (A 5)); hence we write

$$\phi(p, y, t) = \left(-\frac{\cos\gamma}{p + \mathrm{i}\sin\gamma} + \frac{\mathrm{i}}{2}\tan\gamma\right) y + pt + \lambda_{reg}(p)y, \tag{3.3}$$

with $\lambda_{reg}(p)$ admitting a regular Taylor expansion around $-\mathrm{i}\sin\gamma$, such that $\lambda_{reg}(-\mathrm{i}\sin\gamma) = 0$ and convergent on C. (Technically, this requires that $\sin\alpha < 1 - \sin\gamma$,

which we assume to be true here. This condition simplifies the discussion, though the results derived below hold even if this condition is not verified. In fact, it is possible to modify C to encircle separately the singularities at $-\mathrm{i}\sin\gamma$ and $\mathrm{i}\sin\alpha$. Around the latter, the result is given by Cauchy's theorem, whereas around the former we have a calculation similar to the one presented above but involving Lommel's V functions. Identities linking Lommel's U and V functions show that the result is identical.)

$$\lambda_{reg}(p-\mathrm{i}\sin\gamma)y = y\sum_{n=1}^{\infty}\alpha_n(\gamma)p^n. \tag{3.4}$$

Let $\Delta\omega = \sin\alpha + \sin\gamma$ be the difference between the frequency of the approaching wave and the critical frequency. Then

$$\psi_C = \frac{\exp\left[-\mathrm{i}\left(t\sin\gamma - \frac{y}{2}\tan\gamma\right)\right]}{2\pi\mathrm{i}}\int_{\tilde{C}}\frac{\exp\left(p-\frac{\cos\gamma}{p}ty\right)}{p-\mathrm{i}\Delta\omega t}\exp[\lambda_{reg}(p/t-\mathrm{i}\sin\gamma)y]\,\mathrm{d}p, \tag{3.5}$$

where $\tilde{C}$ is the image of C under the shift $p\to(p-\mathrm{i}\sin\gamma)$ followed by the rescaling $p\to p/t$. Furthermore, we have

$$\lambda_{reg}(p/t-\mathrm{i}\sin\gamma)y = \frac{y}{t}\sum_{n=1}^{\infty}\alpha_n(\gamma)\frac{p^n}{t^{n-1}}, \tag{3.6}$$

uniformly convergent on $\tilde{C}$.

From (3.5) and (3.6) we postulate that ψ_C depends on two similarity variables, ξ being the strength of the essential singularity expressed as $\xi^2 \equiv yt\cos\gamma$ and $\delta^2 \equiv y\cos\gamma/t$ (the factor $\cos\gamma$ is introduced for convenience) measuring the departure from unity of $\mathrm{e}^{y\lambda_{reg}(p)}$ and if near criticality (i.e. $\Delta\omega \ll 1$, the case of obvious interest here) a slow time $\Delta\omega t$. We define the near-wall region as the region in the (y,t) plane corresponding to the region $\delta \ll 1$ in the (ξ,δ) plane. For the time being, we assume complete similarity (Barenblatt 1996) in the variable δ in the near-wall region just defined (the existence of complete similarity will be established in Appendix C). Thus, within the near-wall region we have

$$\psi_C \simeq \lim_{\delta\to 0}\psi_C. \tag{3.7}$$

Normalized with the normal component of the wavenumber of the incoming wave μ^+, the near-field region just defined corresponds to the region

$$\mu^+ y \ll \left(\frac{\cos 2\gamma}{\cos\gamma\sin 2\gamma} + O(\Delta\omega)\right)t. \tag{3.8}$$

Over a few buoyancy periods, this region grows to several wavelengths. Indeed, for oceanic (i.e. small) values of γ, this usually encompasses the entire water column. However, even for larger values of γ, which are typically employed in laboratory experiments, the growth is so rapid that for all practical purposes $\delta \ll 1$ does not represent a severe constraint.

Leaving the technical details to Appendix C, we find that

$$\psi_C = \frac{\exp\left[-\mathrm{i}\left(t\sin\gamma - \frac{y}{2}\tan\gamma\right)\right]}{2\pi\mathrm{i}} \int_{\tilde{C}} \frac{\exp\left[\xi\left(\frac{p}{\xi} - \frac{\xi}{p}\right)\right]}{p - \mathrm{i}\Delta\omega t}\,\mathrm{d}p + O(\delta^2)$$
$$= \exp(\mathrm{i}\tilde{x} - \mathrm{i}t\sin\gamma)\mathscr{U}_0(2t\Delta\omega, 2\xi) + O(\delta^2), \qquad \tilde{x} = x + \frac{\tan\gamma}{2}y, \tag{3.9}$$

where

$$\mathscr{U}_0(w, z) \equiv U_0(w, z) + \mathrm{i}U_1(w, z) \tag{3.10}$$

and the U's are Lommel's U function of two variables (See Appendix F and Watson 1995, p. 537). Regarding the four integrals I_1 to I_4, application of standard techniques shows that they contribute a 'ringing' at the buoyancy frequency which is $o(\delta^2)$ (Appendix D), and thus even of less importance in the near field than the terms neglected in (3.9).

Incidentally, the result in (3.9) could have been obtained directly if a long-wave assumption $\nabla^2 \simeq \partial^2/\partial\hat{y}^2$ had been made in (2.1). Indeed, in this case it is easy to verify that $\lambda(p) = -\cos\gamma/(p + \mathrm{i}\sin\gamma)$ and $\lambda_{reg}(p) = -\mathrm{i}(\tan\gamma)/2$ (this approximation is equivalent to assuming a hydrostatic dynamics only if it is applied to a set of coordinates in which gravity is parallel to $\hat{y}$. Also, the x-derivative on the right-hand side of (2.1) cannot be ignored). Conversely, $\partial/\partial y \simeq 1/\delta\partial/\partial\xi$, and the long-wave approximation $\partial^2/\partial y^2 \gg \partial^2/\partial x^2$ holds within the $\delta \ll 1$ region.

3.2. *Buoyancy in the near field*

The buoyancy field satisfies the initial value problem

$$\frac{\partial b}{\partial t} = \sin\gamma\frac{\partial\Psi}{\partial y} - \cos\gamma\frac{\partial\Psi}{\partial x}, \qquad b(x, y, t = 0) = 0. \tag{3.11}$$

Substituting the expression for the streamfunction derived above, after some algebra that uses properties of the $\mathscr{U}$ functions discussed in Appendix F, we obtain

$$b = A\exp[\mathrm{i}(\tilde{x} - t\sin\gamma)]\left\{\left(\frac{2\cos^2\gamma - \sin^2\gamma}{2\sin\alpha\cos\gamma}\right)(\mathscr{U}_0(2t\sin\gamma, 2\xi)\right.$$
$$\left. - \mathscr{U}_0(2\Delta\omega t, 2\xi)) + \mathrm{i}\frac{\sin 2\gamma}{2\sin\alpha}\left(\frac{\mathscr{U}_1(2\Delta\omega t, 2\xi)}{\Delta\omega} - \frac{\mathscr{U}_1(2t\sin\gamma, 2\xi)}{\sin\gamma}\right)\right\} + O(\delta^2) \tag{3.12}$$

which, together with

$$\Psi = A\exp[\mathrm{i}(\tilde{x} - t\sin\gamma)]\mathscr{U}_0(2\Delta\omega t, 2\xi) + O(\delta^2) \tag{3.13}$$

completes the description of the reflected wave in the near-field region to $O(\delta^2)$. This is the form of the solution that will be used in the following sections to (i) understand how the steady-state Phillips solution is recovered as time goes by in the non-critical case, (ii) calculate a solution for a localized beam and (iii) investigate where and when the solution engenders unstable conditions.

4. Approach to steady state near criticality ($0 < |\Delta\omega| \ll 1$)

The existence of complete similarity in the near-wall region has made possible to derive a non-trivial compact expression for the streamfunction and buoyancy field of the reflected wave. It can be easily calculated numerically to provide details of how the reflected wave evolves in time. However, Lommel's functions are sufficiently

ψ	u	$\partial u/\partial y$
$\mathrm{i}\left(\dfrac{\delta}{\Delta\omega}\right) J_{-1}(2\xi)$	$-\mathrm{i}\dfrac{\cos\gamma}{\Delta\omega} J_0(2\xi)$	$\mathrm{i}\left(\dfrac{\cos\gamma}{\Delta\omega}\right)^2 \dfrac{J_1(2\xi)}{2\xi} 2\Delta\omega t$

TABLE 1. Leading-order terms of the transient for along-slope velocity, shear and buoyancy in the $\delta \ll \Delta\omega$ region. All terms are multiplied by the common factor $A\exp[\mathrm{i}(\tilde{x} - t\sin\gamma)]$, and thus oscillates at the critical frequency, regardless of the criticality of the forcing. Only $O(\Delta\omega^{-1})$ terms are indicated for clarity. The terms are written to emphasize the role of the 'slow' time $\Delta\omega t$. The transient of the streamfunction decays as $(\Delta\omega t)^{-1}$; the transient of the along-slope velocity remains constant, while the transient of the shear actually grows as $\Delta\omega t$.

characterized that it is possible to consider the relationship between our solution and the steady-state solution in the near-critical case $0 < |\Delta\omega| \ll 1$ analytically.

The textbook solution for the reflected wave when $\Delta\omega \neq 0$ (see e.g. Phillips 1966) is

$$\Psi^T = A\exp[\mathrm{i}(x + t\sin\alpha + \mu^- y)],\ \mu^- = \frac{1}{2}\frac{\sin 2\gamma - \sin 2\alpha}{\sin^2\gamma - \sin^2\alpha} = \frac{\cos\gamma}{\Delta\omega} + \frac{\tan\gamma}{2} + O(\Delta\omega), \tag{4.1}$$

and

$$b^T = A\frac{\mu^-\sin\gamma - \cos\gamma}{\sin\alpha}\exp[\mathrm{i}(x + t\sin\alpha + \mu^- y)], \tag{4.2}$$

where we have used for μ^- an expression consistent with the long-wave approximation. To establish the asymptotic behaviour of our solution at large time, we note that when $w \gg z$ (see Appendix F),

$$\mathscr{U}_n(w, z) = \mathrm{i}^{-n}\exp\{\mathrm{i}[w/2 + z^2/(2w)]\} + \mathrm{i}\left(\frac{z}{w}\right)^{1-n} J_{n-1}(z) + \cdots. \tag{4.3}$$

Thus, when $\xi < |\Delta\omega|t$, corresponding to $\delta < |\Delta\omega|$,

$$\Psi = A\left\{\exp[\mathrm{i}(x + \mu^- y + t\sin\alpha)] + \mathrm{i}\exp[\mathrm{i}(\tilde{x} - t\sin\gamma)]\frac{\delta}{\Delta\omega}J_{-1}(2\xi)\right\} + O\left(\frac{\delta^2}{\Delta\omega^2}\right). \tag{4.4}$$

The first term is the Phillips streamfunction, while the second term dominates the transient response in the region $\delta < |\Delta\omega|$. Note that the latter oscillates at the critical frequency, regardless of the frequency of the incoming beam. Since $|J_{-1}(z)| \leqslant 1$, the Phillips streamfunction approximates the solution in the region $\delta \ll |\Delta\omega|$. Physically, this is consistent with the fact that the group velocity $-\mathrm{d}p/\mathrm{d}\lambda|_{p=\mathrm{i}\sin\alpha} = \Delta\omega^2/\cos\gamma$. Hence, the line $\delta = |\Delta\omega|$ in the (y, t) plane marks the trajectory of an observer that, travelling at the group velocity, at $t = 0$ leaves the reflecting wall. However, a straightforward calculation (see table 1) shows that the velocity and buoyancy described by the Phillips solution approximate the solution in the *smaller* region $\xi \gg 1$ and $\delta \ll |\Delta\omega|$ (figure 3). That is, in the immediate proximity of the boundary the Phillips solution alone does not describe the along-slope velocity. Finally, and perhaps even more surprisingly, the Phillips solution never provides a good approximation for the shear and buoyancy gradient as they grow in time, linearly along lines of constant ξ, or as $t^{1/4}$ at y fixed. Table 1 summarizes the behaviour of the transient terms.

It would be tempting to ascribe the rather surprising behaviour of the unsteady solution as a consequence of operating under hard ramp-up conditions. In fact, as

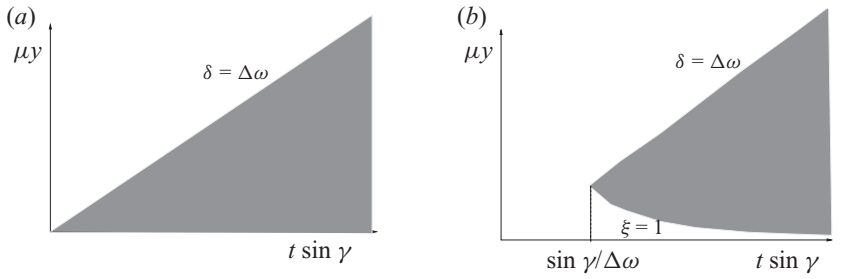

FIGURE 3. Sketch of the region in the (y, t) plane where the Phillips solution for a plane wave reflecting off a sloping boundary agrees to leading order in δ with the evolving solution (3.13). The shaded area in (a) shows the region of agreement for the streamfunction, while in (b) it shows the corresponding region for the along-boundary velocity $u = \partial\Psi/\partial y$. Shear and buoyancy are never found in agreement. We assume near criticality ($|\Delta\omega| \ll 1$) and that a range $|\Delta\omega| \ll \delta \ll 1$ exists.

shown in Appendix E, this is not the case. Even when not at criticality, there is a transient (but long-lived!) response at the critical frequency that prevents the uniform convergence of velocity and shear within the $\delta \ll |\Delta\omega|$ region. This behaviour can be readily understood if we return for a moment to the dynamics as described by the Euler equations, which at the wall assume the particularly simple form

$$\frac{\partial b}{\partial t} - \sin\gamma\, u = 0 \tag{4.5}$$

$$\frac{\partial u}{\partial t} + \sin\gamma\, b = -\frac{\partial P}{\partial x}, \tag{4.6}$$

that can be combined to form the equation for a forced harmonic oscillator

$$\frac{\partial^2 u}{\partial t^2} + \sin^2\gamma\, u = -\frac{\partial^2 P}{\partial x \partial t}. \tag{4.7}$$

For a forcing pressure field oscillating at a given (non-critical frequency) $\sin\alpha$, a *particular* solution can be found, $u_p \sim \exp(\mathrm{i}\sin\alpha)$, corresponding to the Phillips solution. However, in general, a forced harmonic oscillator starting from rest responds both at the forcing frequency and at its natural frequency. This is exactly what happens here, where near the wall the solution has components oscillating at both frequencies. Precisely at the wall the ringing at the natural frequency never goes away, whereas off the wall dispersive effects (mediated by the wall normal velocity) eventually cause the ringing to fade. Likewise, the wall shear (which in the long wavelength limit $\partial^2/\partial y^2 \gg \partial^2/\partial x^2$ coincides with vorticity) obeys a similar harmonic oscillator dynamics. Driven by u and b, which force the shear at both critical and non-critical frequencies, it responds as a harmonic oscillator forced at criticality, albeit the growth occurs on a time scale that expressed in critical frequency periods is $O(\sin\gamma/|\Delta\omega|)$, and thus potentially long.

5. Reflection of a beam

The unbounded (in the along-slope direction) waves discussed in the sections above, while highlighting some interesting aspects of the inviscid reflection process, are of little practical value. Much more interesting is the reflection of a beam of finite width, which can be realized experimentally (Mercier *et al.* 2010) while maintaining

the property of being a solution to both the linearized and fully nonlinear Euler equations (Tabaei & Akylas 2003). We assume a dominant non-dimensional along-slope wavelength equal to 1 and use a Witch of Agnesi of width $2L$ to localize the beam in the direction perpendicular to the group velocity of the beam (sharper localizing functions can be considered as well, provided that they have a finite number of simple poles when extended to the complex plane). The Fourier transform of $S(x)$ (see (2.4)), the beam projection along the boundary, is

$$S(k) = \frac{L}{2}\,\mathrm{e}^{-|(k-1)|L}. \tag{5.1}$$

We assume $L \geqslant \pi$, so that the beam width contains at least one wavelength. The small amount of upward-propagating wavelengths contained in $S(k)$ (i.e. the fraction with $k<0$) is not of concern here, since they contribute a term $O(\mathrm{e}^{-L})$ to the streamfunction, and thus negligible. The contribution from the positive wavenumbers is

$$\Psi = \frac{AL}{2}\frac{\exp(\mathrm{i}(\tilde{x}-t\sin\gamma))}{2\pi\mathrm{i}}\int_{\tilde{C}}\frac{\exp\left(pt-\dfrac{\cos\gamma}{p}y\right)}{p-\mathrm{i}\Delta\omega} \left[\frac{1}{L-\mathrm{i}\left(\tilde{x}+\mathrm{i}\dfrac{\cos\gamma}{p}y\right)}+\frac{1-\exp\left(-L-\mathrm{i}\tilde{x}+\dfrac{\cos\gamma}{p}y\right)}{L+\mathrm{i}\left(\tilde{x}+\mathrm{i}\dfrac{\cos\gamma}{p}y\right)}\right]\mathrm{d}p, \tag{5.2}$$

(we retain the $O(\mathrm{e}^{-L})$ term within the square brackets to cancel an exponential divergence) and from here onward we dispense from indicating the $O(\delta^2)$ remainder. The contour integral can be easily calculated to give

$$\Psi = A\left\{\frac{\mathscr{U}_0(2\Delta\omega t,2\xi)}{1+\dfrac{(x+\mu^- y)^2}{L^2}}+\mathrm{i}\frac{L}{2}\frac{y\cos\gamma}{\Delta\omega}\left[\frac{\mathscr{U}_0(2\mathrm{i}\xi^2/(L-\mathrm{i}\tilde{x}),2\xi)}{(L-\mathrm{i}\tilde{x})(\mathrm{i}(x+\mu^- y)-L)} +\frac{\mathscr{V}_2(-2\mathrm{i}\xi^2/(L+\mathrm{i}\tilde{x}),2\xi)}{(L+\mathrm{i}\tilde{x})(\mathrm{i}(x+\mu^- y)+L)}\right]\right\}\exp\mathrm{i}(\tilde{x}-t\sin\gamma). \tag{5.3}$$

(See Appendix F for a definition of $\mathscr{V}$. The recurrence relationship for $\mathscr{U}$ and $\mathscr{V}$ is used to write the solution in terms of $\mathscr{U}_0$.) The first term in the square brackets is the outgoing wave beam, which is nothing but the localized version of the streamfunction obtained earlier. As we have seen, at large times this term contributes the freely propagating Phillips solution, within the wedge $\delta \ll |\Delta\omega|,\ \xi \gg 1$, as well as transients both near the leading edge and near the reflecting boundary. The terms within the square brackets add a near-wall transient which is absent in the unlocalized case. The

latter can be rewritten as

$$\Psi_{tr} = \frac{AL}{2}\mathrm{i}\xi^2 \left[\frac{\exp\left(-\dfrac{\xi^2}{L-\mathrm{i}\tilde{x}} + L - \mathrm{i}\tilde{x}\right) - \mathrm{i}\mathscr{U}_1(-2\mathrm{i}(L-\mathrm{i}\tilde{x}), 2\xi)}{(L-\mathrm{i}\tilde{x})(\mathrm{i}\xi^2 + t\Delta\omega(\mathrm{i}\tilde{x} - L))} \right.$$

$$\left. - \frac{\mathrm{i}\mathscr{U}_1(2\mathrm{i}(L+\mathrm{i}\tilde{x}), 2\xi)}{(L+\mathrm{i}\tilde{x})(\mathrm{i}\xi^2 + t\Delta\omega(\mathrm{i}\tilde{x} + L))} \right] \exp \mathrm{i}(\tilde{x} - t\sin\gamma). \quad (5.4)$$

5.1. *Critical case: unlocalized versus beam*

It is instructive, at this point, to consider how, in the critical case $\Delta\omega = 0$, localization affects the reflection process. In the unlocalized limit, the streamfunction assumes the particularly simple form

$$\Psi = A\exp[\mathrm{i}(\tilde{x} - t\sin\gamma)]J_0(2\xi). \quad (5.5)$$

Aside from the factor $\mathrm{e}^{\mathrm{i}y\tan\gamma/2}$, this coincides with the solution that DY obtained. The largest growth rate for the along-slope velocity $u = \partial\Psi/\partial y$ and shear $S = \partial^2\Psi/\partial y^2$ are found at the boundary, where they increase as t and t^2 respectively. However, both quantities diverge, albeit at the slower rate of $t^{1/4}$ and $t^{3/4}$ respectively, even away from the boundary. As remarked by earlier, at the wall the behaviour is essentially similar to an oscillator forced at its resonant frequency.

The behaviour for a localized beam is different. While at the boundary u and S diverge as in the unlocalized case, away from the boundary both quantities, after an initial period of growth, *decay* in time. Indeed, according to (5.4) when $y \gg (L^2 + (x + y\tan\gamma/2)^2)/t\cos\gamma$,

$$u = -AL^2\exp(\mathrm{i}(\tilde{x} - t\sin\gamma))\frac{J_3(2\xi)}{\xi^3}t\cos\gamma + \cdots \quad (5.6)$$

and

$$S = AL^2\exp(\mathrm{i}(\tilde{x} - t\sin\gamma))\frac{J_4(2\xi)}{\xi^4}(t\cos\gamma)^2 + \cdots . \quad (5.7)$$

Figure 4 shows the transient-induced along-slope velocity at the centre of the beam at $k_0\hat{y} = 0.1$. In the critical case, the time scale of the transient coincides with the buoyancy time scale. The shallower the angle of the slope, the wider the gulf between the buoyancy time scale and the period of the waves. Hence, the decay occurs sooner for shallow slopes than for steeper slopes.

6. Shear and overturning

The most obvious experimental effect of near-critical reflection is the generation of strong mixing near the boundary in localized regions near the boundary. A comprehensive stability analysis even of our simplified solution is beyond the scope of the present paper. Rather, following Thorpe (1987) and DY, we will use established criteria to explore which of the possible routes to instability, shear or overturning, our solution is likely to take within the near-field region. As a definition of overturning

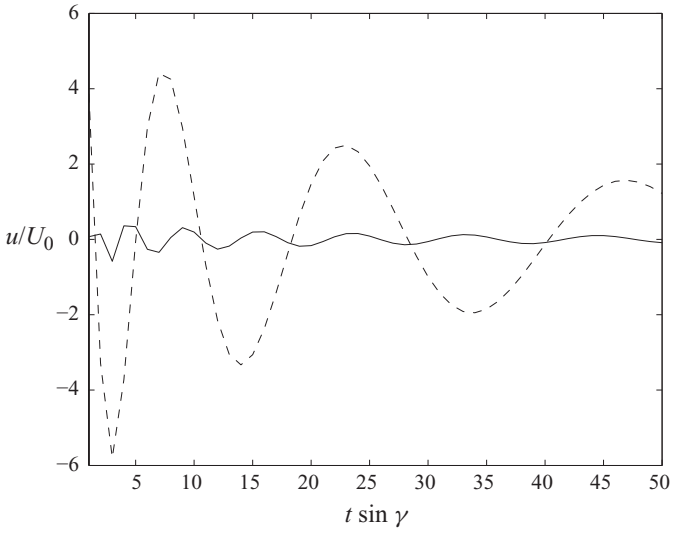

FIGURE 4. Along-slope velocity at $t \sin\gamma = 1, 2, \ldots$ measured at the centre of the beam at $k_0\hat{y} = 0.1$. The slope of the boundary is 3° for the solid line and 15° for the dashed line. In both cases the velocity is normalized with the maximum along-slope velocity in the *incoming* beam and $k_0\hat{L} = \pi$

we take the occurrence of the region of the negative local Brunt–Väisälä frequency

$$N^2 = 1 - \frac{\partial}{\partial\zeta}(b_{inc} + b) < 0, \tag{6.1}$$

while for shear instabilities we assume a simple test based on the local Richardson number

$$J = \frac{N^2}{S^2} < \frac{1}{4},\ S = -\mathrm{Re}\frac{\partial}{\partial\zeta}(\Psi_{inc} + \Psi). \tag{6.2}$$

In general, where and when the stratification overturns or is overcome by shear will depend now on the amplitude of the incoming wave A, departure from criticality $\Delta\omega$ and slope angle γ.

As was shown by Thorpe (1987), as the amplitude of a freely propagating wave approaches a finite value A_c, the maximum slope of the isopycnals locally approaches infinity, and the wave experiences localized overturning. The fact that the wave always reaches overturning with $J > 1/4$ is due to the fact that the regions where the wave buoyancy field is most effective at weakening the background stratification coincide with the regions of zero shear. Expressed differently, the condition is that shear and buoyancy are $\pi/2$ out of phase, that is, they are in quadrature. However, once transient effects are taken into consideration, quadrature between shear and buoyancy gradient is established at best only asymptotically in time; hence, regions of waning stratification do not necessarily coincide with regions of low shear before the asymptotic phase difference sets in. Thus, we can have the possibility that initially, and within the region affected by the transient, regions where shear instability is possible may occur. Contrast this to DY's solution, whose buoyancy gradient is always in quadrature with the along-slope shear, and in this respect resembles a freely propagating waves. Hence, DY find that in their solution, waves always overturn first (like free waves).

6.1. *Small amplitude waves*

The maximum isopycnals slope of a reflected Phillips wave is

$$a_{max}^{ref} = a_{max}^{inc} \left(\frac{\sin(\alpha - \gamma)}{\sin(\alpha + \gamma)} \right)^2. \tag{6.3}$$

When $a_{max}^{ref} < 1$, overturning, if present, is due to interactions between the incoming and outgoing waves in the overlapping region and/or transient effects. A necessary condition for the former to occur is $a_{max}^{ref} + a_{max}^{inc} > 1$, and since close to criticality $a_{max}^{ref} \gg a_{max}^{inc}$, the latter condition is met only if the reflected wave itself is close to overturning. The contribution from the transient, in contrast, can generate small statically unstable regions even for very weak waves. For the along-slope velocity (5.4) shows that close to the boundary a beat develops between the outgoing beam, which contributes a term oscillating at the frequency of the incoming beam

$$u_{beam} \simeq \frac{L^2}{L^2 + x^2} \frac{\cos\gamma}{\Delta\omega} \exp(\mathrm{i}(x - t\sin\alpha)) \tag{6.4}$$

and the contribution from the transients which adds a term

$$u_{trans} \simeq \frac{L^2}{L^2 + x^2} \frac{\cos\gamma}{\Delta\omega} \left(\frac{x}{L^2 + x^2} - \mathrm{i} \right) \exp(\mathrm{i}(x - t\sin\gamma)), \tag{6.5}$$

oscillating at the critical frequency. The first term is an effect of the localization of the beam, whereas the second term is due to the inherently tendency of (2.1) to generate shear discussed earlier. For very wide beams, the contribution from the localization in the latter expression vanishes, and one recovers the non-localized form of the transient. However, for localized beams, this causes the largest along-slope velocities to preferentially occur near the shoulders of the beam (figure 5). A similar argument applies to shear and buoyancy. This results in a modulation of J over a time scale $O(2\pi/\Delta\omega)$. To summarize, even very weak waves can generate unstable conditions, due entirely to transient effects, though nonlinearly generated harmonics, which are completely neglected in our solution, could modify the outcome. This could happen if, for example, higher harmonics of the type considered by Tabaei *et al.* (2005) sap energy from the base flow.

6.2. *Intermediate waves*

When the reflected waves are close to overturning, transients can induce localized overturning in a sizable region off the wall. This is an interesting case, because the incoming wave is still too weak to give any significant contribution. As for weak waves, this is due entirely by the non-Phillips terms in the solution. However, in this case we observe the formation of isolated regions of overturned fluid which develop off the boundary and are advected by the phase velocity towards the wall, where they eventually merge with the unstable regions at the wall (figure 6). Near the wall, the unstable regions first appear as regions where $0 < J < 1/4$, though they quickly evolve a core of statically unstable fluid ($N^2 < 0$), as opposed to the off-wall unstable regions which always start as statically unstable, and appear sooner, usually within the end of the first wave cycle.

6.3. *Large waves*

The unstable regions which appear during the reflection process of weak waves are confined to a limited region near the boundary. It is therefore reasonable to assume

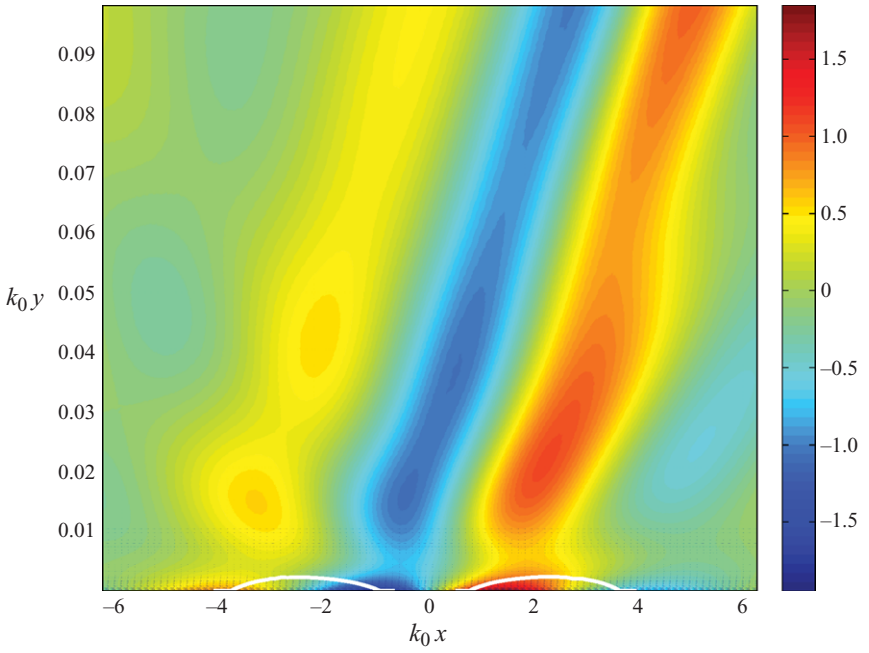

FIGURE 5. (Colour online) Along-slope velocity (normalized with the maximum along-slope velocity of the reflected Phillips wave) and instable regions in a weak wave at $t \sin\gamma/2\pi = 25.5$. The white lines enclose the unstable region, which is comprised of a overturning core surrounded by a ring where the local Richardson number is below critical. The slope is $\gamma = 15°$, $\Delta\omega/\sin\gamma = -.1$ and $L = \pi$. The maximum slope of the reflected Phillips wave isopycnals is 0.2.

that the analytic solution should hold outside these regions, possibly with minor modifications.

For sufficiently large incoming waves, such that

$$a_{max}^{\text{inc}} \geqslant \left(\frac{\sin(\alpha+\gamma)}{\sin(\alpha-\gamma)}\right)^2, \tag{6.6}$$

the reflected Phillips wave itself is statically unstable; thus, we expect that the analytic solution should provide at best an indication of where, when and what type of instabilities should occur first. When the incoming waves themselves are not close to overturning (i.e. $a_{max}^{inc} \ll 1$) we find that the unstable regions appear first close to the boundary, where generally $J < 1/4$, since the time t_c that lapses before the onset is $O(\Delta\omega^{-1})$ over a wide range of slope angles and thus, unstable regions develop before the local phase difference between buoyancy and shear approaches $\pi/2$ (i.e. they are not yet in quadrature). For a given slope γ, the dependence of the time t_c required for unstable regions to develop near criticality is in qualitative agreement with the experiments of De Silva *et al.* (1997). Quantitatively, our solution seems to go unstable sooner. This could be due, most likely, to lacking viscous effects, both near the wall and in the interior of the fluid, suppressing (or at least retarding) the onset of measurable instabilities. Often, the region where at first $J < 1/4$ is observed becomes very rapidly an overturning regions. However, we find examples in which the shear-unstable region expands before any overturning is observed. In all cases, the region is localized. When the unstable region is primarily static (i.e. $J < 1/4$ becomes

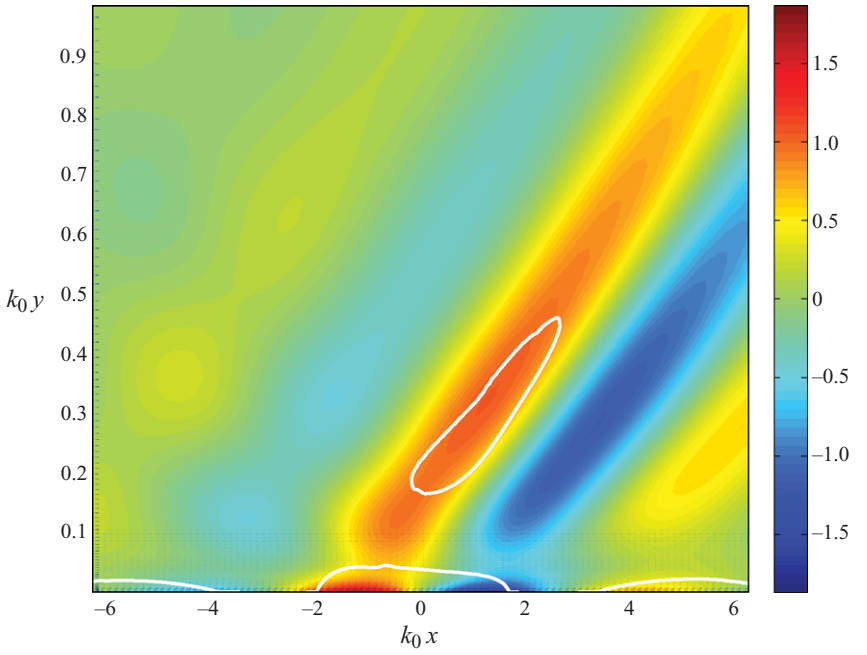

FIGURE 6. (Colour online at http://journals.cambridge.org/flm) Along-slope velocity (normalized with the maximum along-slope velocity of the reflected Phillips wave) and unstable regions in an intermediate wave at $t \sin\gamma/2\pi = 3$. The white lines enclose the unstable region, which is comprised of a overturning core surrounded by a ring where the local Richardson number is below critical. In addition to the unstable region near the wall, we now have isolated regions of statically unstable fluid forming off the wall. Note also the difference in the vertical scale. The slope $\gamma = 15°$, $\Delta\omega/\sin\gamma = -0.5$ and the maximum slope of the reflected Phillips wave is 0.84.

rapidly $J < 0$) the statically unstable region at the wall coincides with the region of diverging flow, whereas primarily $0 < J < 1/4$ regions occur near the regions of maximum along-slope velocity. If we calculate the solution past the onset of unstable regions at the wall, we can observe isolated regions of overturning which first appear *away* from the wall, and move closer to the wall in the subsequent evolution, often merging with unstable regions coming from the wall. Whereas for the unstable regions close to the wall it is the intense shear generated by the reflected wave that drives the region unstable, in the latter case it is the buoyancy anomaly of the reflected field that causes overturning. The more supercritical the wave is, these off-wall, detached overturned regions develop the sooner, in accordance with the observations of De Silva *et al.* (1997), and are absent in subcritical waves. This and the longer time (in critical frequency units) for instabilities to develop are the major differences between supercritical and subcritical reflection. This isolated overturning regions are sometime found above the the region of the field described by the Phillips solution, especially when γ is small. When the amplitude of the incoming waves is close to overturning unstable regions can occur initially away from the wall, as regions where $0 < J < 1/4$, as a wave–wave interaction of the edge transient with the incoming wave.

7. Discussion and summary

In this paper, we have shown that the linearized reflection of internal waves from a sloping boundary can be described in the time domain by a solution that

is well behaved even when the slope of the reflector is critical, in fact analytic in $\Delta\omega = \sin\alpha + \sin\gamma$. Within the near-wall region $y \ll t$ (figure 3) the solution can be approximated in a closed form in terms of Lommel's functions of two variables. The textbook Phillips solution is achieved in the subregion $\Delta\omega^2 t/\cos\gamma > y > 1/t\cos\gamma$. The upper bound reflects the finite group velocity $\Delta\omega^2/\cos\gamma$ at which the waves propagate. Below this region, the flow is affected by a transient at the critical frequency $\sin\gamma$, which combines with the steady solution on frequency $\sin\alpha$ to create regions of enhanced shear. Within the latter transient region, shear-unstable regions can develop even under very weak incoming waves, when the superposition of the incoming and outgoing Phillips waves is expected to be stable. The solution can be easily localized to a physically realizable beam, with similar properties. Finally, the streamfunction in the closed form recovers the leading-order solution obtained by matched asymptotic by DY, even though we did not include nonlinear effects. The equivalence does not extend to the buoyancy field, which in DY is always in quadrature with the velocity field. So, while in the DY solution the unstable regions are always convective (local $N^2 < 0$), in our solution we observe both shear and convective unstable regions. Nonetheless, the connection is significant, because it shows that nonlinearity, at least in the weak form considered by DY, is not going to alter the basic tendency of the reflection process to create fine scale shear.

In our analysis, we have neglected entirely the effects of viscosity and diffusivity on the momentum and buoyancy field. As shown by DY, a thin viscous boundary layer near the reflector can be introduced to accommodate the no-slip condition at the wall. However, here we have shown that the generation of fine scale shear is a basic property of the reflection dynamics. Even within the inviscid, outer solution, in a finite time shear will reach scales at which it becomes necessary to consider the viscosity of the fluid. It is reasonable to expect that at oceanic scales instabilities will develop earlier, but in the laboratory this may not always be the case, and further work is needed to elucidate the effects of viscosity outside the viscous wall sublayer.

Comparison of the analytic solution with fully nonlinear simulations is the focus of an ongoing effort. In particular, it will be interesting to see if and how instabilities will change the properties of the outgoing beam, especially under weak incoming waves, for which a stable outgoing Phillips solution is expected.

I wish to dedicate this work to the memory of Professor O. M. Phillips (1931–2010), who introduced me to the world of stratified flows. I would like to thank S. Sarkar and E. Santilli for engaging discussions on the subject. This work was supported by NSF grant OCE-0825997.

Appendix A. Complex plane extensions of $\lambda(p)$

Zeros of complex-coefficient second-order polynomial equations typically contain square roots of algebraic expressions of the coefficients. In general, this implies that if $\lambda(p)$ is a root of the polynomial associated with (2.6) on a given open set U of $\mathbb{C}$, by analytic continuation we can obtain multiple extensions of the same root. In this appendix, we derive the two extensions of the same root, which are used in the paper.

Let $z = x + \mathrm{i}y$ be a complex number. We define the square root of z as

$$\sqrt{z} = |z|^{1/2}\exp(\mathrm{i}\mathrm{Arg}(z)/2), \tag{A 1}$$

where $|z| = x^2 + y^2$ and $-\pi < \mathrm{Arg}(z) < \pi$. With this choice of the branch cut (the

negative real axis), $\mathrm{Re}\sqrt{z} \geqslant 0$, and the real part is continuous across the cut. Furthermore, if z and w are complex numbers with positive real part, then $\sqrt{zw} = \sqrt{z}\sqrt{w}$. It then follows that if $\mathrm{Re}\, p > 0$, then $p\sqrt{1+p^2} = p^2\sqrt{1+p^{-2}}$.

Having established these basic properties, it is easy to show that on the open set $U = \{p \in \mathbb{C} : \mathrm{Re}\, p > 0\}$,

$$\lambda_{ff}(p) = \frac{\mathrm{i}\sin\gamma\cos\gamma - p^2\sqrt{1+\frac{1}{p^2}}}{p^2 + \sin^2\gamma}, \tag{A 2}$$

and

$$\lambda_{nf}(p) = \frac{\mathrm{i}\sin\gamma\cos\gamma - p\sqrt{1+p^2}}{p^2 + \sin^2\gamma}, \tag{A 3}$$

are equivalent expressions of the same zero of the characteristic equation associated with (2.6) with negative real part, hence $A(p)\mathrm{e}^{\lambda(p)y}$ with $\lambda(p)$ given by either (A 2) or (A 3) and $A(p)$ an arbitrary holomorphic function on U, is a solution to (2.6) which satisfies the boundary condition at $y = \infty$. Thus, either expression can be used in lieu of $\lambda(p)$ in (2.10). $\lambda_{ff}(p)$ can be analytically continued to the rest of the complex plane with a branch cut $\{p \in \mathbb{C} : |\mathrm{Im}\, p| \leqslant 1,\ \mathrm{Re}\, p = 0\}$ (it is left to the reader to verify that $1 + p^{-2}$ indeed maps the branch cut into the negative real axis). Extended in this way, $\lambda_{ff}(p)$ admits a Laurent expansion centered at the origin, convergent for $|p| > 1$, whose first few terms are

$$\lambda_{ff}(p) = -1 - \frac{\mathrm{e}^{-2\mathrm{i}\gamma}}{2p^2} + O(p^{-4}). \tag{A 4}$$

$\lambda_{nf}(p)$ instead can be continued with a branch cut $\{p \in \mathbb{C} : |\mathrm{Im}\, p| \geqslant 1,\ \mathrm{Re}\, p = 0\}$ (which again is mapped to the negative real axis by the argument of the square root). The extended $\lambda_{nf}(p)$ has a simple pole at $-\mathrm{i}\sin\gamma$, the critical frequency, and the corresponding Laurent expansion, convergent on $|p + \mathrm{i}\sin\gamma| < 1 - \sin\gamma$, is

$$\lambda_{nf}(-\mathrm{i}\sin\gamma + p) = -\frac{\cos\gamma}{p} + \frac{\mathrm{i}}{2}\tan\gamma - \frac{1}{4}\frac{1+\cos^2\gamma}{\cos^3\gamma}p + O(p^2). \tag{A 5}$$

This pole becomes an essential singularity of $\mathrm{e}^{\phi(p,y,t)}$ and will be instrumental in determining the behaviour of the solution in the near-field solution.

Even though they are obviously not identical functions over $\mathbb{C}$ minus the respective branch cut, either one returns the same streamfunction when used to calculate the inverse Laplace transform integral in (2.9), since the latter is evaluated on a contour entirely contained within the open set U where the two extensions coincide. Which one to choose then becomes a matter of convenience. In practice, the location of the critical points $\mathrm{d}\phi/\mathrm{d}p = 0$ determines which one to use. For large values of y/t, the critical points are located away from the origin, and thus it is expedient to have an extension with a Laurent series convergent for large values of $|p|$. Conversely, when y/t is small, the critical points are to be found near the singularity, and it is very convenient not having to deal with singularities on a branch cut.

Appendix B. The streamfunction in the far-field region, $y > t$

We use the method of steepest descend to calculate (2.9). We set in (2.10) $\lambda \equiv \lambda_{ff}(p)$ with $\lambda_{ff}(p)$ given by (A 2). When $\bar{\delta} \equiv y/t > 1$, from (A 4) the critical points where

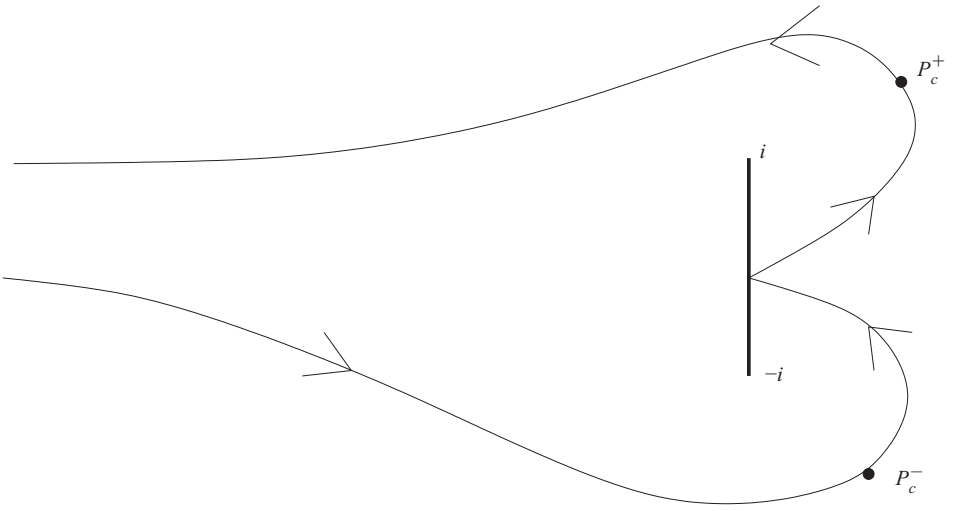

FIGURE 7. The integration contour in the far-field case. Note that in this case the branch cut (thick line) stretches between $-i$ and i. On the right-hand side of the branch cut the path terminates at the singularity at $p = -\mathrm{i}\sin\gamma$, which is used to switch the phase.

$\mathrm{d}\phi/\mathrm{d}p = 0$ are

$$p_c^\circ = -\overline{\delta}^{1/3}(\exp(-2\mathrm{i}\gamma/3) + O(\overline{\delta}^{-1})),\ p_c^\pm = \overline{\delta}^{1/3}(\exp(\mathrm{i}(-2\gamma \pm \pi)/3) + O(\overline{\delta}^{-1})). \quad \text{(B 1)}$$

It is a matter of simple algebra to show that the steepest descent path at $p_c^\pm$ is locally given by $p_c^\pm + s\exp\mathrm{i}(-\gamma \mp \pi)/3$. To evaluate the integral, we deform it as shown in figure 7. The path follows the line of the constant phase $\mathrm{Im}(\phi(p_c^-))$ which starts from $-\infty + \mathrm{i}\mathrm{Im}(\phi(p_c^-))/t$, climbs the saddle point at p_c^- and then descends on the opposite side to the singular point located at $p = -\mathrm{i}\sin\gamma$ (where $\mathrm{Re}\,\phi \sim -\cos\gamma/(p + \mathrm{i}\sin\gamma)$), from which it re-emerges along the path of the constant phase $\mathrm{Im}(\phi(p_c^+))$ to climb the saddle point at p_c^+, descending then to $-\infty + \mathrm{i}\mathrm{Im}(\phi(p_c^+))/t$ (note that $\mathrm{Im}(\phi(p_c^-)) < 0 < \mathrm{Im}(\phi(p_c^+))$). The leading-order contribution of each saddle point is

$$\frac{\exp(-t\overline{\delta}(1 - \overline{\delta}^{-2/3}\Phi(\theta_c)) - \mathrm{i}\theta_c/2)}{\sqrt{6\pi t\rho}}, \quad \text{(B 2)}$$

where $\theta_c = \mathrm{Arg}(p_c)$ and $\Phi(\theta_c) = 3\,\mathrm{e}^{\mathrm{i}\theta_c}/2$. The leading-order contribution does not depend on the frequency of the incoming wave. The medium acts as a low-pass filter. The above relationship is uniformly valid with the exclusion of the region $\{(y,t)\ :\ t < y, t > 1/\sqrt{y}\}$ which is entirely included in the $t < 1$ region, which is excluded from our analysis. The last relationship thus shows that in the region $y > t$ the streamfunction vanishes exponentially, as expected on physical grounds.

Appendix C. The contribution of the integration along C to the streamfunction

Here we present a more rigorous derivation of the right-hand side of (3.9). First, we notice the obvious fact that

$$f(z) \equiv \int_C \frac{\mathrm{e}^{\phi(p,y,t)}}{p - \mathrm{i}z}\,\mathrm{d}p, \quad \text{(C 1)}$$

as a function of the complex argument z is holomorphic within the region of the complex plane enclosed by C. Let

$$\exp(y\lambda_{reg}(p - \mathrm{i}\sin\gamma)) = \sum_{n=0}^{\infty} \beta_n(\gamma, y)p^n \tag{C 2}$$

be the power series expansion of $\mathrm{e}^{y\lambda_{reg}(p)}$, which exists and converges uniformly on C. Then

$$\mathrm{e}^{\phi(p,y,t)} = \exp\left(\left(-\frac{\cos\gamma}{p + \mathrm{i}\sin\gamma} + \frac{\mathrm{i}}{2}\tan\gamma\right)y + pt\right)\sum_{n=0}^{\infty}\beta_n(\gamma, y)(p + \mathrm{i}\sin\gamma)^n, \tag{C 3}$$

and

$$\frac{1}{2\pi\mathrm{i}}\int_C \frac{\mathrm{e}^{\phi(p,y,t)}}{p - \mathrm{i}\sin\alpha}\,\mathrm{d}p = \frac{\exp\left(-\mathrm{i}(t\sin\gamma - \frac{y}{2}\tan\gamma)\right)}{2\pi\mathrm{i}} \sum_{n=0}^{\infty}\beta_n(\gamma, y)\int_{\tilde{C}} \frac{\exp\left(pt - \dfrac{\cos\gamma}{p}y\right)}{p - \mathrm{i}\Delta\omega}p^n\,\mathrm{d}p, \tag{C 4}$$

where $\tilde{C}$ is the image of the C under the shift $p \to p - \mathrm{i}\sin\gamma$. We are allowed to exchange summation with integration since the series converges uniformly on $\tilde{C}$. Each integral can be evaluated in terms of $\mathscr{U}$ functions (see Appendix F) to give

$$\frac{1}{2\pi\mathrm{i}}\int_C \frac{\mathrm{e}^{\phi(p,y,t)}}{p - \mathrm{i}\sin\alpha}\,\mathrm{d}p = \exp(\mathrm{i}(\tilde{x} - t\sin\gamma))\sum_{n=0}^{\infty}\beta_n(\gamma, y)(\Delta\omega)^n\mathscr{U}_{-n}(2t\Delta\omega, 2\xi). \tag{C 5}$$

The right-hand side of (C 5) inherits the holomorphic character of the left-hand side, from which it follows that for $\Delta\omega$ within $\tilde{C}$ a unique expansion exists

$$\exp(\mathrm{i}(\tilde{x} - t\sin\gamma))\sum_{n=0}^{\infty}\beta_n(\gamma, y)(\Delta\omega)^n\mathscr{U}_{-n}(2t\Delta\omega, 2\xi) = \sum_{n=0}^{\infty}a_n(\Delta\omega)^n. \tag{C 6}$$

From the definition of the $\mathscr{U}$ functions, re-arranging the terms appropriately, we have

$$a_n = \left(\frac{\mathrm{i}}{\delta}\right)^n\sum_{m=0}^{\infty}\delta^m\beta_m(\gamma, y)J_{n-m}(2\xi), \tag{C 7}$$

with ξ and δ defined earlier. It is trivial to show that if $|\delta| < 1 - \sin\gamma$, the series that appears in the definition of the each coefficient a_m is uniformly convergent (the region within which the Taylor expansion of $\exp(y\lambda_{reg}(p - \mathrm{i}\sin\gamma))$ converges is independent of y and Bessel's functions are bounded). Thus, carrying the first two terms, and keeping in mind that $y = \xi\delta/\cos\gamma$ and β_n is an overall $O(\delta)$ finite sum of powers of δ,

$$\begin{aligned} a_n &= \left(\frac{\mathrm{i}}{\delta}\right)^n(J_n(2\xi) + \delta\beta_1(\gamma, y)J_{n-1}(2\xi) + O(\delta^3)) \\ &= \left(\frac{\mathrm{i}}{\delta}\right)^n\left(J_n(2\xi) - \delta^2\frac{1}{4}\frac{1 + \cos^2\gamma}{\cos^4\gamma}\xi J_{n-1}(2\xi) + O(\delta^3)\right). \end{aligned} \tag{C 8}$$

Substituting and calculating the remaining series we obtain

$$\frac{1}{2\pi \mathrm{i}}\int_C \frac{\mathrm{e}^{\phi(p,y,t)}}{p-\mathrm{i}\sin\alpha}\,\mathrm{d}p = \mathscr{U}_0(2\Delta\omega t, 2\xi) + \delta^2\frac{1}{4}\frac{1+\cos^2\gamma}{\cos^4\gamma}(t\Delta\omega)\mathscr{U}_{-1}(2\Delta\omega t, 2\xi) + O(\delta^3). \tag{C 9}$$

We leave to the reader to show that to $O(\delta^3)$ a more compact expression equivalent to the one above is

$$\frac{1}{2\pi \mathrm{i}}\int_C \frac{\mathrm{e}^{\phi(p,y,t)}}{p-\mathrm{i}\sin\alpha}\,\mathrm{d}p = \mathscr{U}_0(2\Delta\omega(1-\alpha\delta^2), 2\xi\sqrt{1-\alpha\delta^2}) + O(\delta^3),\ \alpha = \frac{1}{4}\frac{1+\cos^2\gamma}{\cos^4\gamma}. \tag{C 10}$$

Appendix D. Contribution from the integrals along the branch cuts

The contribution to the streamfunction along the upper branch cut is

$$\frac{1}{2\pi \mathrm{i}}\int_{I_1+I_2} \frac{\mathrm{e}^{\phi(p,y,t)}}{p-\mathrm{i}\sin\alpha}\,\mathrm{d}p = \frac{\mathrm{e}^{\mathrm{i}t}}{2\pi \mathrm{i}}\int_0^\infty \frac{\mathrm{e}^{\lambda_+(s)y}-\mathrm{e}^{\lambda_-(s)y}}{(1+s)-\sin\alpha}\,\mathrm{e}^{\mathrm{i}st}\,\mathrm{d}s \equiv \frac{\mathrm{e}^{\mathrm{i}t}}{2\pi \mathrm{i}}\int_0^\infty h(s)\,\mathrm{e}^{\mathrm{i}st}\,\mathrm{d}s, \tag{D 1}$$

where

$$\lambda_\pm(s) = \frac{\mathrm{i}\sin\gamma\cos\gamma \pm (1+s)\sqrt{s(2+s)}}{\sin^2\gamma-(1+s)^2}. \tag{D 2}$$

Since

$$\frac{\mathrm{d}h}{\mathrm{d}s} = s^{-1/2}\exp(-\mathrm{i}y\tan\gamma)y\left(\frac{\sqrt{2}}{(\sin\alpha-1)\cos^2\gamma}+O(s)\right), \tag{D 3}$$

with the bracketed part being regular, an integration by parts followed by the application of standard formulae (Erdélyi 1956, p. 48) gives

$$\frac{\mathrm{e}^{\mathrm{i}t}}{2\pi \mathrm{i}}\int_0^\infty h(s)\,\mathrm{e}^{\mathrm{i}st}\,\mathrm{d}s = \frac{\mathrm{e}^{\mathrm{i}t}}{2\pi t}\int_0^\infty \frac{\mathrm{d}h}{\mathrm{d}s}\,\mathrm{e}^{\mathrm{i}st}\,\mathrm{d}s = \frac{\exp(\mathrm{i}(t+\pi/4-y\tan\gamma))}{\sqrt{2\pi}(1-\sin\alpha)\cos^2\gamma}\frac{y}{t^{3/2}} + o(t^{-3/2}). \tag{D 4}$$

Adding the contribution from the lower branch cut, obtained in a similar way, we obtain

$$-\frac{\exp(-\mathrm{i}y\tan\gamma)}{\sqrt{2\pi}\cos^2\gamma}\frac{y}{t^{3/2}}\left(\frac{\exp(\mathrm{i}(t+\pi/4))}{1-\sin\alpha}-\frac{\exp(-\mathrm{i}(t+\pi/4))}{1+\sin\alpha}\right)+o(t^{-3/2}). \tag{D 5}$$

Note that this contribution is a modulated wave at the buoyancy frequency, whose modulation is $O(\delta^{5/2})$ and thus negligible.

Appendix E. The streamfunction under soft start-up

Omitting the factor $A\exp\mathrm{i}\tilde{x}$ for simplicity,

$$\begin{aligned}\frac{\partial\psi^h}{\partial\sin\alpha} &= \exp(-\mathrm{i}t\sin\gamma)t\left[\mathscr{U}_{-1}(2\Delta\omega t, 2\xi)+\left(\frac{\xi}{\Delta\omega t}\right)^2\mathscr{U}_1(2\Delta\omega t, 2\xi)\right]\\ &= \mathrm{i}t\exp\left(\mathrm{i}\left(t\sin\alpha+\frac{\cos\gamma}{\Delta\omega}y\right)\right)+\mathrm{i}\exp(-\mathrm{i}t\sin\gamma)\frac{\delta}{\Delta\omega^2}J_1(2\xi)+O((\delta/\Delta\omega)^2).\end{aligned} \tag{E 1}$$

valid for $t\Delta\omega \gg \xi$ (i.e. $\delta \ll \Delta\omega$). Restoring all factors, and assuming that $t > \tau$, to leading order

$$\psi^s = A\left[\exp(\mathrm{i}(x + \mu^- y + t\sin\alpha)) + \exp(\mathrm{i}(\tilde{x} - t\sin\gamma))\frac{\delta}{\Delta\omega}J_1(2\xi)\frac{1-\exp(\mathrm{i}\tau\Delta\omega)}{\tau\Delta\omega}\right], \tag{E 2}$$

which has the same converge properties of ψ^h.

Appendix F. Some useful relations concerning $\mathscr{U}$

Lommel introduced the functions U and V that now bear his name (not to be confused with the solutions to Lommel's differential equation) to study the refraction of light waves off a circular aperture (von Lommel 1884–1886). Here we give a derivation of $\mathscr{U}$ and discuss some useful properties such as integral relationships, connection to Lommel's V functions and recursion relationships. The first and so far probably the only application of these functions to problems of wave propagation outside optics can be found in Pocklington (1905), who considered a 'toy' mechanical problem with some elements in common to the problem at hand, namely that the group velocity is anti-parallel to the phase velocity.

F.1. *$\mathscr{U}$ and Lommel's functions of two variables*

To establish the connection between $\mathscr{U}$ and Lommel's functions, we start with the well-known expansion (Watson 1995, p. 14)

$$\exp(\xi(p/\delta - \delta/p)) = \sum_{n=-\infty}^{\infty} \mathrm{J}_n(2\xi)p^n\delta^{-n}, \tag{F 1}$$

where J_n is the Bessel function of integer order n. It follows that if C is any closed contour which contains both the origin and is,

$$\begin{aligned}\frac{1}{2\pi\mathrm{i}}\int_C \frac{\exp(\xi(p/\delta - \delta/p))}{p - \mathrm{i}s}p^m\,\mathrm{d}p &= \sum_{n=-\infty}^{\infty}\sum_{l=0}^{\infty}\delta^{-n}(\mathrm{i}s)^l\mathrm{J}_n(2\xi)\frac{1}{2\pi\mathrm{i}}\int_C p^{n-l-1+m}\,\mathrm{d}p \\ &= s^m\sum_{l=0}^{\infty}\left(\frac{\delta}{s}\right)^{m-l} i^l\mathrm{J}_{l-m}(2\xi) \\ &= s^m\sum_{l=0}^{\infty}\left(\frac{\mathrm{i}s\xi\delta^{-1}}{\xi}\right)^{2l-m}\left(\mathrm{J}_{2l-m}(2\xi) + \mathrm{i}\frac{s\xi\delta^{-1}}{\xi}\mathrm{J}_{2l+1-m}(2\xi)\right) \\ &= s^m(U_{-m}(2s\xi\delta^{-1}, 2\xi) + \mathrm{i}U_{-m+1}(2s\xi\delta^{-1}, 2\xi)).\end{aligned} \tag{F 2}$$

Note that the rather cavalier attitude displayed above (and below as well) in exchanging the order of summation and integration is justified by the fact that power series converge uniformly within any compact subset contained within the convergence radius. For a detailed description of Lommel's functions and their properties the reader is referred to Chapter 16.5 of Watson (1995).

F.2. *Sundry relationships concerning $\mathscr{U}_n$ and $\mathscr{V}_n$*

The following relationships for $\mathscr{U}_n(w, z)$ and $\mathscr{V}_n(w, z)$ can be derived easily. A useful recurrence formula is

$$\mathscr{U}_n(w, z) = \mathrm{i}\left(\frac{w}{z}\right)^{n-1}\mathrm{J}_{n-1}(z) - \mathrm{i}\,\mathscr{U}_{n-1}(w, z), \tag{F 3}$$

with its counterpart for $\mathscr{V}$ functions

$$\mathscr{V}_{n+1}(w,z) = \mathrm{i}\mathscr{V}_n + \left(\frac{w}{z}\right)^{1-n} \mathrm{J}_{1-n}(z). \tag{F 4}$$

The following relationship links $\mathscr{V}$ and $\mathscr{U}$:

$$\mathscr{V}_n(w,z) = \mathscr{U}_{2-n}(w,z) + \exp\left(\mathrm{i}\left(\frac{w}{2} + \frac{z^2}{2w} + n\frac{\pi}{2}\right)\right). \tag{F 5}$$

Practically speaking, U is obtained if the contour C in (F 2) includes both the essential singularity at the origin and the pole at is, whereas one obtains $\mathscr{V}$ if C includes only the essential singularity.

A useful relation links the derivative of the function at order n with the function at order $n+1$ according to

$$\frac{\partial}{\partial z}\mathscr{U}_n(w,z) = -\frac{z}{w}\mathscr{U}_{n+1}(w,z), \tag{F 6}$$

useful to calculate the along-slope velocity and shear. Finally, the following reciprocating formulae hold:

$$\mathscr{U}_n(w,z) = \exp\left(\mathrm{i}\left(\frac{w}{2} + \frac{z^2}{2w} - n\frac{\pi}{2}\right)\right) - \mathrm{i}(-)^n\mathscr{U}_{1-n}\left(\frac{z^2}{w}, z\right), \tag{F 7}$$

$$\mathscr{V}_{2-n}(w,z) = -\mathrm{i}(-)^n\mathscr{U}_{1-n}\left(\frac{z^2}{w}, z\right). \tag{F 8}$$

The demonstrations are left to reader.

F.3. *An alternative expression for* $\mathscr{U}_n$

When regarded as a function of complex variables, $\mathscr{U}_n(w,z)$ is an entire function in z. If $n \geqslant 0$, it is also entire in w, having a pole of order $-n$ for $n<0$. However, if $\mathrm{Im}\, s \neq 0$ in (F 2), the series defining $\mathscr{U}_n$ may converge slowly, and thus be of little computational use. In this case, it is better to use Borel's theory of summation to evaluate $\mathscr{U}_n$. For simplicity, we consider the case $n=0$. For different values of n, the calculation can be easily modified, or, for $|n|$ not too large, the recurrence relationship (F 3) can be used. Let u : $\mathrm{Re}\, u > 0$ and c be a contour that includes the origin but not u. Consider the integral

$$\begin{aligned}
\frac{1}{2\pi\mathrm{i}}\int_c \frac{\mathrm{e}^{pt-\frac{y}{p}}}{p-u}\,\mathrm{d}p &= -\sum_{m=0}^{\infty}\frac{1}{2\pi\mathrm{i}}\int_c \frac{p^m}{u^{m+1}}\,\mathrm{e}^{pt-\frac{y}{p}}\,\mathrm{d}p \\
&= -\frac{1}{2\pi\mathrm{i}}\sum_{m=0}^{\infty}\int_0^{\infty}\mathrm{e}^{-zu}\frac{z^m}{m!}\,\mathrm{d}z\frac{\partial^m}{\partial t^m}\int_c \mathrm{e}^{pt-\frac{y}{p}}\,\mathrm{d}p \\
&= -\int_0^{\infty}\mathrm{e}^{-zu}\sum_{n=0}^{\infty}\frac{z^m}{m!}\frac{\partial^m}{\partial t^m}\left[\mathrm{J}_{-1}(2\sqrt{yt})\sqrt{\frac{y}{t}}\right]\mathrm{d}z \\
&= -\int_0^{\infty}\mathrm{e}^{-zu}\left(\mathrm{J}_{-1}(2\sqrt{y(t+z)})\sqrt{\frac{y}{t+z}}\right)\mathrm{d}z,
\end{aligned} \tag{F 9}$$

where the reader will recognize that the bracketed term in the last line is the Borel transform of the series in the first line. Because of the rapidly decreasing exponential factor, the last integral can be evaluated numerically with ease. If instead u : $\mathrm{Re}\, u < 0$,

a similar argument can be repeated, but using a contour that includes both u and the origin, and using derivatives with respect to y to express p^{-n}. This exercise is left to the reader.

REFERENCES

Arnold, V. I. & Khesin, B. A. 1998 *Topological Methods in Hydrodynamics*. Springer.

Barenblatt, G. I. 1996 *Scaling, Self-Similarity and Intermediate Asymptotics*. Cambridge University Press.

Cacchione, D.A. & Drake, D. E. 1986 Nepheloid layers and internal waves over continental shelves and slopes. *Geo. Mar. Lett.* **16**, 147–152.

Cacchione, D. A., Pratson, L. F. & Ogston, A. S. 2002 The shaping of continental slopes by internal tides. *Science* **296**, 724–727.

Cacchione, D. A. & Wunsch, C. 1974 Experimental study of internal waves on a slope. *J. Fluid Mech.* **66**, 223–239.

Dauxois, T. & Young, W. R. 1999 Near-critical reflection of internal waves. *J. Fluid Mech.* **390**, 271–295.

De Silva, I. P. D., Imberger, J. & Ivey, G. N. 1997 Localized mixing due to a breaking internal wave ray at a sloping bed. *J. Fluid Mech.* **350**, 1–27.

Dickson, R. R. & McCave, I. N. 2002 Nepheloid layers on the continental slope west of Porcupine Bank. *Deep-Sea Res.* **33**, 797–818.

Erdélyi, A. 1956 *Asymptotic Expansions*. Dover.

Gostiaux, L., Dauxois, T., Didelle, H., Sommeria, J. & Viboud, S. 2006 Quantitative laboratory observations of internal wave reflection on ascending slopes. *Phys. Fluids* **18**, 056602, doi:10.1063/1.2197528.

Ivey, G. N. & Nokes, R. I. 1989 Vertical mixing due to the breaking of critical internal waves on sloping boundaries. *J. Fluid Mech.* **204**, 479–500.

Kistovich, Yu. V. & Chashechkin, Yu. D. 1995 The reflection of beams of internal gravity waves at a flat rigid surface. *J. Appl. Math. Mech.* **59** (4), 579–585.

Legg, S. & Adcroft, A. 2003 Internal wave breaking at concave and convex continental slopes. *J. Phys. Oceanogr.* **33**, 2224–2246.

von Lommel, E. C. J. 1884–1886 Die beugungserscheinungen einer kreisrunden oeffnung und eines kreisrunden schirmchens theoretisch und experimentell bearbeitet. *Abh. der Math. Phys. Classe der k. b. Akad. der Wiss. (Mnchen)* **15**, 229–328.

MacIntyre, S. 1998 Turbulent mixing and resource supply to phytoplankton. In *Physical Processes in Lakes and Oceans, Coastal Estuarine Studies* (ed. J. Imberger), vol. 54, pp. 561–590. AGU.

McPhee-Shaw, E. E. 2006 Boundary-interior exchange: reviewing the idea that internal-wave mixing enhances lateral dispersal near continental margins. *Deep-Sea Res.* **43**, 42–59.

McPhee-Shaw, E. E. & Kunze, E. 2002 Boundary layer intrusions from a sloping bottom: a mechanism for generating intermediate nepheloid layers. *J. Geophys. Res.* **107** (C6), 3050.

Mercier, M., Martinand, D., Mathur, M., Gostiuax, L., Peacock, T. & Dauxois, T. 2010 New wave generation. *J. Fluid Mech.* **657** 308–334.

Moum, J. N., Caldwell, D. R., Nash, J. D. & Gunderson, G. D. 2002 Observations of boundary mixing over the continental slope. *J. Phys. Ocean.* **32**, 2113–2130.

Nash, J. D., Kunze, E., Toole, J. & Schmitt, R. 2004 Internal tide reflection and turbulent mixing on the continental slope. *J. Phys. Oceanogr.* **34**, 117–1134.

Phillips, O. M. 1966 *The Dynamics of the Upper Ocean*. Cambridge University Press.

Pocklington, H. C. 1905 Growth of a wave-group when the group velocity is negative. *Nature* **71**, 607–608.

Slinn, D. N. & Riley, J. J. 1998 Turbulent dynamics of a critically reflecting internal gravity wave. *Theor. Comput. Fluid Dyn.* **11**, 281–303.

Sobolev, S. L. 1954 On a new problem of mathematical physics. *Izvestiya USSR Acad. Sci., Ser. Mat.* **18**, 3–50.

Staquet, C. & Sommeria, J. 2002 Internal gravity waves: from instabilities to turbulence. *Annu. Rev. Fluid Mech.* **34**, 559–593.

Tabaei, A. & Akylas, T. R. 2003 Nonlinear internal gravity beams. *J. Fluid Mech.* **482**, 141–161.

Tabaei, A., Akylas, T. R. & Lamb, K. G. 2005 Nonlinear effects in reflecting and colliding internal wave beams. *J. Fluid Mech.* **526**, 217–243.

Thorpe, S. A. 1987 On the reflection of a train of finite-amplitude internal waves from a uniform slope. *J. Fluid Mech.* **178**, 279–302.

Venayagamoorthy, S. K. & Fringer, O. B. 2006 Numerical simulations of the interaction of internal waves with a shelf break. *Phys. Fluids* **18**, 076603.

Watson, G. N. 1995 *A Treatise on the Theory of Bessel Functions*. Cambridge University Press.

Wunsch, C. 1968 On the propagation of internal waves up a slope. *Deep-Sea Res.* **25**, 251–258.

Wunsch, C. 1969 Progressive internal waves on slopes. *J. Fluid Mech.* **35**, 131–144.